JISSN 1330-3651 (Print), ISSN 1848-6339 (Online) https://doi.org/10.17559/TV-20240831001958
Original scientific paper

Innovative Vibration Signal Recognition for Enhanced Pipeline Safety Using Optimized Wavelet Denoising and Particle Swarm-Tuned Neural Networks

Fang WANG*, Caijun XU, Bin LIU, Wenjun CHEN, Shaodong YAN

Abstract: The precision of vibration signal recognition is critical in the safety monitoring of long-distance pipelines. This paper introduces an advanced methodology for signal classification that integrates wavelet denoising with particle swarm optimization (PSO), to enhance the accuracy of signal recognition and restoration. A novel wavelet parameter selection technique is proposed, which significantly refines the denoising process. Additionally, PSO is employed to fine-tune the initial weights and thresholds of a BP neural network, serving as the classifier in this study. The input data, collected from a long-distance pipeline simulation system under various vibration scenarios, resulted in a dataset of xx samples. Each signal is processed using wavelet denoising and MATLAB computation, resulting in 22 feature values used as inputs for the classifier. The findings demonstrate that the optimized BP neural network achieves a recognition accuracy of 97.5%, with a performance improvement of 13.53%. This methodology aligns well with the future direction of intelligent pipeline systems, providing substantial support for enhancing pipeline safety monitoring. The practical industrial significance of this research is its potential to significantly enhance the accuracy of vibration signal processing in long-distance pipeline transportation systems. With the implementation of optimized BP neural networks, pipeline operators can more accurately detect and identify potential safety hazards, such as cracks, enabling earlier warning and intervention. This improvement in detection accuracy is crucial for maintaining the structural integrity of pipelines, minimizing downtime, and preventing environmental contamination, thus offering a powerful solution for enhancing operational safety and reliability in pipeline systems.

Keywords: BP neural network; feature extraction; Particle swarm optimization algorithm; Wavelet denoising

1 INTRODUCTION

In the context of oil and natural gas transportation, pipelines have long been recognized as the most effective and reliable means due to their superior safety, cost-effectiveness, consistent performance, and minimal environmental impact. This makes them a fundamental component of the energy sector. However, as pipelines age and the risks associated with geological hazards, material corrosion, and human activities increase, global concern regarding the increasing frequency of pipeline failures has intensified. The consequences of such failures are severe, posing significant threats to the safety, property, and environment of nearby communities. According to data referenced in [1], there are approximately 640 pipeline incidents reported annually, leading to 14 fatalities and 57 injuries on average. Among the various causes, third-party damage has been identified as a major factor contributing to pipeline ruptures and leaks [2].

The imperative for regular pipeline status inspections is essential to maintaining the safety and reliability of pipeline operations.

Diverse detection technologies, including Electromagnetic Ultrasonic Guided Wave (EUGW), suffer from signal attenuation, particularly in thick-walled structures or materials with complex geometries, which limits its ability to detect deep-seated defects effectively. Additionally, the sensitivity of EUGW to small surface cracks or micro-defects is relatively low, and its performance can be significantly degraded by environmental factors such as temperature variations and electromagnetic interference. Magnetic Flux Leakage (MFL), while effective for detecting large surface or near-surface defects, is primarily applicable to ferromagnetic materials, making it unsuitable for non-magnetic materials like aluminum or composite materials. Furthermore, MFL's sensitivity to small cracks or deep internal defects is limited. Additionally, the accuracy of defect localization may be affected in complex structural geometries, where the leakage patterns are distorted. Eddy Current (EC) detection, although widely used for surface and near-surface crack detection, suffers from limited penetration depth, making it ineffective for detecting defects in thicker materials. Moreover, it is restricted to conductive materials, which means non-metallic or non-conductive materials cannot be assessed using this method. The technique's sensitivity is also highly dependent on the material properties, requiring careful calibration when dealing with different alloys or heterogeneous materials. Microwave detection offers advantages in non-destructive testing of materials without contact, yet its effectiveness diminishes in high-density materials such as metals, where penetration depth is limited. Additionally, the frequency choice is crucial higher frequencies provide better resolution but have limited penetration, while lower frequencies penetrate better but lose resolution. The impact of environmental factors like humidity, temperature, and electromagnetic noise can also significantly affect the stability and reliability of microwave signals, posing challenges for practical implementation. Acoustic Emission (AE) detection, while capable of identifying the initiation of cracks or defects through stress waves, is often challenged by its signal interpretation complexity. AE signals are prone to interference from background noise and vibrations, especially in large structures, which can make it difficult to isolate defect-related signals. Furthermore, the technology's defect localization accuracy is limited, particularly in large or irregular components, where signal distortion or dissipation occurs before reaching the sensor. Each of these technologies has its unique strengths but also inherent limitations that need to be addressed for broader industrial application. Their sensitivity, penetration depth, material compatibility, and susceptibility to environmental noise are key challenges that researchers continue to explore in order to enhance the effectiveness and applicability of non-destructive testing.

This study provides insights into the operational status

of oil and gas pipelines by analyzing detected signals. Traditional manual analysis methods can no longer meet the current stringent requirements for pipeline safety assessments. Hence, the quest for accurate, efficient, and reliable analysis and processing of pipeline signals has become a critical area of research in oil and gas pipeline status detection technology [9]. A key challenge in signal analysis is overcoming the limitations of traditional time-domain and frequency-domain methods. Time-domain methods fail to capture the full details of signals, while frequency-domain methods, such as Fast Fourier Transform (FFT) and Short-Term Fourier Transform (STFT), struggle with non-stationary signals and suboptimal time-frequency resolution [10, 12].

The Fast Fourier Transform (FFT), while a powerful tool for analyzing stationary signals, exhibits significant limitations when applied to non-stationary signals, where the frequency content evolves over time. Since FFT assumes a stationary signal over the entire analysis window, it fails to capture time-varying frequency components, making it unsuitable for signals like speech or seismic events. For example, in speech signal analysis, where the frequency components shift rapidly as different phonemes are spoken, FFT provides only an overall averaged frequency spectrum, neglecting the temporal evolution of the speech signal. This loss of time-dependent information limits its utility in speech recognition and other applications requiring precise temporal features. Furthermore, FFT fails to indicate the timing of specific frequency components, which is critical for signals with transient events. In seismic signal analysis, FFT would fail to identify the precise timing of seismic events, such as an earthquake or fault slip, as it averages the frequency content over the entire signal duration, missing key temporal characteristics of the transient events.

On the other hand, the Short-Time Fourier Transform (STFT) attempts to address the time-varying nature of non-stationary signals by segmenting the signal into short time windows and performing FFT on each segment. However, STFT suffers from a trade-off between time and frequency resolution, as defined by the Heisenberg uncertainty principle. Narrow time windows offer good frequency resolution but poor time resolution, while wider windows provide better time resolution but poor frequency resolution. This trade-off can significantly impact the analysis of signals with rapidly changing frequency components. For instance, in musical signal analysis, where both transient and sustained sounds coexist, a short time window would fail to accurately resolve overlapping frequency components, such as a rapidly oscillating note and a sustained harmonic. Conversely, using a long window to improve frequency resolution would blur the time localization of the transient events, making it difficult to precisely determine when the frequency shift occurs. Similarly, in fault detection in rotating machinery, where faults such as bearing failures generate sudden, transient vibrations with sharp frequency shifts, STFT with a fixed window may not capture these brief events effectively, resulting in an inaccurate diagnosis and delayed response to machinery malfunctions.

Wavelet transform, with its ability to localize signal characteristics in both time and frequency domains, emerges as a superior tool, offering advantages such as non-redundancy, orthogonality, and ease of implementation [13].

Amidst the plethora of signal recognition and classification methods, artificial intelligence, notably Artificial Neural Networks (ANN) and Support Vector Machines (SVM), have become prominent in signal processing [14]. This article adopts the Backpropagation Neural Network (BPNN) algorithm for signal recognition, a method previously employed successfully by scholars to address practical problems in diverse fields. For example, Qiu et al. [15] used an Improved Particle Swarm Optimization (IPSO)-BPNN to predict the demand for agricultural machinery spare parts, solving data classification issues in this domain. Liu et al. [16] enhanced the BP neural network by replacing the hidden layer node transfer function with a wavelet basis function, creating a Wavelet Neural Network (WNN) to address algorithm convergence problems. Kong et al. [17] calculated the power spectral density (PSD) to extract features and then constructed a BPNN classifier for recognizing and classifying radar echo signals.

Despite these advancements, challenges persist, such as the difficulty in selecting optimal wavelet parameters, the ongoing need to enhance classifier performance Signal-to-noise ratio limitations, real-time processing requirements and environmental interference factors. In actual pipeline monitoring, signals can be disturbed by various noises, such as mechanical noise, electromagnetic interference, or natural ambient noise, which can significantly reduce the signal-to-noise ratio, thus affecting the accuracy of signal processing and identification. This study later develops or improves adaptive filters to adjust and eliminate specific types of noise in real time, thereby improving the signal-to-noise ratio. Many signal processing methods perform well in accuracy, but can be challenging when processing large amounts of data in real time. In emergency situations, such as pipeline leaks or ruptured, rapid identification and response are required, and slow processing algorithms may not meet the needs of real-time monitoring. This study can design and train lightweight neural network models that require fewer computational resources, which speeds up processing and is suitable for real-time data analysis. Pipeline monitoring systems may be subject to interference in harsh environmental conditions, such as extreme temperature, humidity, chemical corrosion, and geological changes. These environmental factors may affect the performance of the sensor and the quality of the signal, thereby reducing the accuracy of the identification of the pipeline status. This study wants to develop sensors that are resistant to the effects of harsh environments to improve the accuracy and reliability of data acquisition. To address these challenges, this article introduces a novel wavelet parameter selection method. Specifically, wavelet denoising is employed to reduce noise in the signal data, improving the accuracy of subsequent analysis. The wavelet transform is used for feature extraction due to its ability to localize signal characteristics in both time and frequency domains. Furthermore, this study utilizes the Particle Swarm Optimization (PSO) algorithm to optimize BPNN parameters, thereby enhancing the performance of the classifier. This combined approach effectively addresses the challenges of wavelet parameter selection and classifier

optimization in signal recognition tasks. The Wavelet Neural Network (WNN) integrates wavelet transforms into neural networks by replacing the traditional activation functions in the hidden layers with wavelet functions, which can capture both time and frequency information of signals, making it suitable for analyzing non-stationary signals such as those encountered in pipeline monitoring. The wavelet parameter selection method systematically evaluates different combinations of wavelet parameters to identify the optimal settings that maximize the performance of the signal recognition task. Wavelet denoising applies the wavelet transform to decompose the signal into different frequency components and, by thresholding the wavelet coefficients, effectively reduces noise while preserving important features of the original signal, which is particularly useful in preprocessing pipeline signals to improve the reliability of subsequent analysis. Particle Swarm Optimization (PSO) is an optimization algorithm inspired by the social behavior of birds flocking or fish schooling and is employed to optimize the parameters of the BPNN, such as weights and biases, by iteratively improving a candidate solution with regard to a given measure of quality. In the context of this research, PSO helps to find the optimal neural network parameters that enhance the classifier's performance in recognizing signal patterns from pipelines.

The proposed approach begins with wavelet denoising to enhance pipeline signal clarity, followed by the application of the PSO algorithm to optimize the BP neural network. Particle swarm optimization (PSO) is a swarm intelligence algorithm that simulates the behavior of bird flocks to solve optimization problems. In traditional BP neural networks, weights and biases are usually initialized randomly, which can cause the network to fall into local optimal solutions. When combining PSO and BP neural networks, each particle represents a set of possible network weights and biases. Particle swarm algorithms are used to search globally for optimal weights and biases, and then use these parameters to initialize the neural network. Next, the BP algorithm is used for local search and fine-tuning to further improve network performance. This approach combining global search and local search can improve the efficiency of network training and reduce the risk of falling into local optimality. This optimization aims to rectify issues of poor localization and generalization in the learning process, ultimately deriving optimal initial weights and thresholds. Subsequently, a classification model is constructed based on the PSO-BP component classifier. The efficacy of this method is demonstrated through the classification of pipeline signal data collected by sensors, offering a robust solution to the identified challenges.

Despite advancements in signal recognition methods, challenges persist. Signal-to-noise ratio limitations arise from mechanical noise, electromagnetic interference, and ambient noise, affecting signal processing accuracy. Real-time processing demands highlight the inefficiency of traditional methods when handling large data volumes, which can hinder rapid response during emergencies such as leaks or ruptures. Additionally, environmental interference factors, including extreme temperatures, humidity, and chemical corrosion, compromise sensor performance and signal quality. These gaps in current research underscore the need for innovative solutions.

To address these challenges, this study introduces a comprehensive approach that combines wavelet denoising, Particle Swarm Optimization (PSO), and Backpropagation Neural Networks (BPNN). Wavelet denoising enhances signal clarity by decomposing signals into frequency components and applying thresholding to reduce noise. PSO optimizes BPNN parameters, improving classifier accuracy and addressing issues of poor localization and generalization in traditional neural networks. The proposed methodology effectively mitigates signal-to-noise ratio issues, accelerates real-time processing through lightweight neural network models, and enhances system resilience in harsh environmental conditions. By bridging these research gaps, this work contributes to the development of a robust and efficient pipeline signal monitoring system, addressing the critical challenges in signal processing and classification for pipeline safety management.

2 SIGNAL DENOISING

The comprehensive pipeline vibration signal recognition process is illustrated in Fig. 1. The original vibration data collected by the pipeline system is obtained from "signal" and the signal is pre-processed in "Smooth Processing" to reduce the short-term fluctuations in the signal and highlight the long-term trend. Then "Denoising" the signal into the filter to reduce random noise, making the signal smoother and easier for subsequent analysis. Then, "Feature Extraction" is used to extract features conducive to recognition and classification from the pre-processed signals. Finally, in the "PSO-BP" step, a neural network model is constructed and optimized by integrating the PSO algorithm with the BP neural network to accurately identify and classify the vibration signals of pipelines [18].

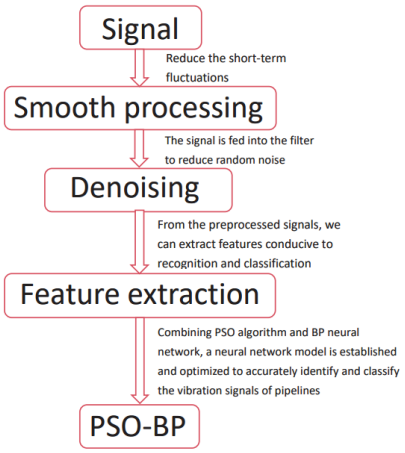

Figure 1 Overall process of pipeline vibration signal recognition

2.1 Wavelet Denoising

Denoising is a crucial preprocessing step in signal processing, significantly enhancing the performance and reliability of signal recognition algorithms. Background noise in pipeline vibration signals can affect the accurate recognition and extract the target features, making it imperative to mitigate noise interference before further signal processing.

The traditional Fourier transform, which uses an infinite-length constant amplitude sine function as a basis function, is effective for analyzing periodic stationary signals but struggles with non-stationary signals [19]. To address this limitation, Morlet introduced wavelet analysis. In this study, we employ the wavelet threshold denoising method to remove noise, aiming to eliminate redundant portions of the signal while amplifying meaningful segments. The essence of wavelet threshold denoising is to suppress noise components while preserving relevant signal features [20]. The wavelet basis function, decomposition levels, threshold, and threshold function directly affect the denoising effectiveness [21]. Soft and hard threshold functions are widely used in threshold denoising [22]. Four primary rules govern the selection of wavelet thresholds: fixed threshold criterion (sqtwolog), unbiased risk estimation criterion (rigrsure), mixed criterion (heursure), and minimax criterion (minimaxi).

Sqtwolog is a method to determine an optimal threshold by calculating an estimate of the noise variance. The core idea of rigrsure method is to select an adaptive threshold by calculating the risk value to minimize the loss in the process of denoising. The advantage of the heursure method is that the threshold can be dynamically adjusted according to the characteristics of the signal and noise. As a conventional threshold selection method, its goal is to select a fixed threshold to minimize the mean square error between the denoised signal and the original signal. The minimaxi method uses a heuristic function to automatically select the optimal threshold; which threshold to use is based on the value of the calculated variable.

Selecting the optimal parameter combination for denoising pipeline vibration signals has been a focal point of research when employing the wavelet threshold denoising algorithm. Extensive experiments have shown that selecting a threshold processing mode in MATLAB that remains constant with noise levels renders the four threshold selection rules and two threshold denoising methods unaffected by the signal denoising outcome. However, when using noise level estimation in the first-layer wavelet decomposition to adjust, the influence of the decomposition scale on denoising effectiveness can be eliminated. Building on this insight, we propose a new parameter selection method:

(1) In MATLAB, select a threshold processing mode that does not change with noise levels. The pipeline vibration signal is decomposed into approximate and detailed components of different scales by 6-layer wavelet decomposition. By using the correlation between the detail component and the approximate component of the signal, the range of the decomposition scale is determined. Determine the decomposition scale between 1 - 6 and identify the wavelet base with the best denoising effect.

(2) Keep the wavelet base and decomposition scale constant and adjust the threshold value according to the noise level estimation of the first layer of wavelet decomposition. Combine the two threshold denoising methods with the four-threshold selection rules and select the combination with the best denoising effect.

(3) Adjust the noise level estimation for each layer of Qo obtain the parameter combination with the best noise removal effect.

The db5 wavelet with a decomposition scale of 1 was found to yield the highest *SNR* (8.8938 dB). The choice was further supported by its superior time-frequency localization and computational efficiency. A sensitivity analysis was conducted to determine the optimal values for population size, inertia weight, and maximum iterations. The selected parameters (population size = 50, inertia weight = 0.7, iterations = 100) demonstrated the best balance between optimization accuracy and convergence speed. The network's structure (2 layers with 10 and 5 nodes) was optimized based on a grid search. This configuration minimized validation errors while avoiding overfitting. The use of ReLU in the hidden layers and softmax in the output layer ensured effective non-linear transformation and classification.

2.2 Method Verification

In this paper, the Signal-to-Noise Ratio (*SNR*) stands out as the chosen evaluation index. A larger *SNR* value signifies a diminished proportion of noise in the signal, indicating superior denoising effects. A higher *SNR* also correlates with heightened similarity between the reconstructed and original signals, indicating improved signal reconstruction accuracy. The existing vibration signal recognition methods may not be effective when the signal-to-noise ratio is low.

Wavelet symmetry is required to ensure that the filter has a linear phase and avoids phase distortion for signal processing. Wavelets are also required to have orthogonality to reduce the correlation and redundancy of wavelet subbands [23]. Building on these principles, this study explores the selection of an optimal wavelet basis function from the dbn (n = 1, 2, ..., 8), symn (n = 1, 2, ..., 8), and coifn (n = 1, 2, 3, 4, 5) wavelet systems. "dbn" is Daubechies wavelet, also called compact supported orthogonal wavelet."symn" refers to the Symlet function, also known as the approximately symmetric compact supported set orthogonal wavelet. "coifn" refers to the Coiflet wavelet. "n" is its wavelet base order. For the pipeline vibration signal under consideration, selecting a decomposition scale greater than 4 results in a negative signal-to-noise ratio. Consequently, the decomposition scale is restricted to 1 - 3. Through MATLAB analysis, the paper scrutinizes the optimal denoising effects achieved by different wavelet bases under varying decomposition scales.

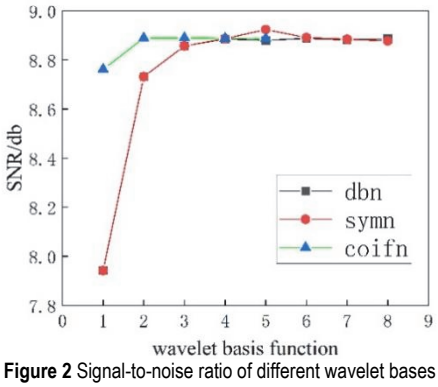

Figure 2 Signal-to-noise ratio of different wavelet bases

At the three selected decomposition scales, the 21 wavelet bases are employed to denoise the original

vibration signal, and the resulting signal-to-noise ratio is computed. In MATLAB, the threshold processing mode that remains constant with noise levels is selected, with the decomposition scale set at 1. The experimental results, illustrated in Fig. 2, highlight that the denoising effect of the db5 wavelet is the most prominent, yielding a signal-to-noise ratio of 8.8938 db.

At a decomposition scale of 2, the signal-to-noise ratio outcomes obtained through various wavelet bases are as follows. It is evident that the coif5 wavelet exhibits the most effective denoising, boasting a signal-to-noise ratio of 8.7967 db.

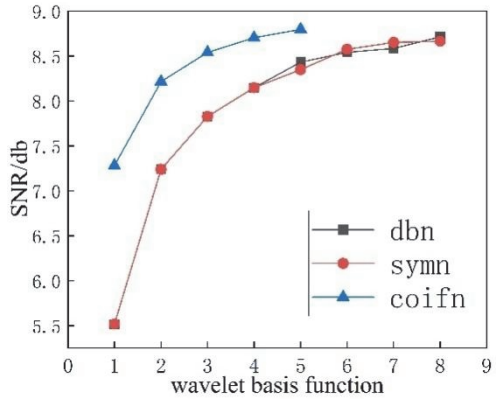

Figure 3 Signal-to-noise ratio of different wavelet bases

When the decomposition scale is 3, the *SNR* results obtained by selecting different wavelet bases are as follows. It can be found that sym8 wavelet has the best denoising effect, and the *SNR* is 3.7637 db.

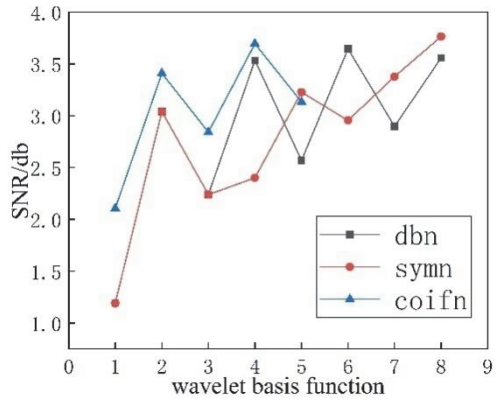

Figure 4 Signal-to-noise ratio of different wavelet bases

The chosen wavelet basis is db5, with the decomposition scale set at 1. In MATLAB, adjustments are performed based on noise level estimation of the first layer of wavelet decomposition.

Table 1 *SNR* and *MSE* under different permutation combinations

	heursure	minimaxi	rigrsure	sqtwolog
SNR Hard threshold	8.8806	8.8795	8.8799	8.8805
SNR Soft threshold	8.8805	8.8840	8.8819	8.8860
MSE Hard threshold	1.5373	1.5358	1.5354	1.5372
MSE Soft threshold	1.5360	1.5360	1.5357	1.5359

Two threshold denoising methods, along with four threshold selection rules, are systematically arranged and combined. The denoising effects are evaluated using the Signal-to-Noise Ratio (*SNR*) index and Signal-to-Noise Ratio (*MSE*). The *SNR* values under various arrangement combinations are presented in Tab. 1. Notably, the combination of the soft threshold and sqtwolog stands out with the most effective denoising, achieving a signal-to-noise ratio of 8.8860 db.

Maintaining the consistency of the wavelet basis and decomposition scale, adjustments are performed in MATLAB using noise level estimation of each layer of wavelet decomposition. The two threshold denoising methods are systematically arranged and combined with the four threshold selection rules. Tab. 2 presents the results, revealing an identical outcome to that of Tab. 1.

Table 2 *SNR* under different permutation combinations

	heursure	minimaxi	rigrsure	sqtwolog
Hard threshold	8.8806	8.8795	8.8799	8.8805
Soft threshold	8.8858	8.8840	8.8819	8.8860

Initially, a fixed threshold is employed to handle the pattern of noise level variation, with the Signal-to-Noise Ratio (*SNR*) serving as the metric for evaluating denoising outcomes. Utilizing 21 distinct wavelet bases and 63 combinations of 3 decomposition scales, the pipeline vibration signal undergoes denoising via wavelet thresholding. The goal is to identify the optimal wavelet basis and decomposition scale. Following this, while maintaining the wavelet basis and decomposition scale, adjustments are made to the threshold processing mode for noise level variation to pinpoint the most effective threshold denoising method and threshold selection rule combination.

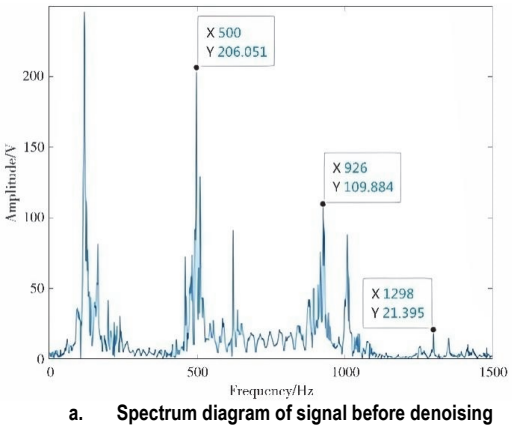

a. Spectrum diagram of signal before denoising

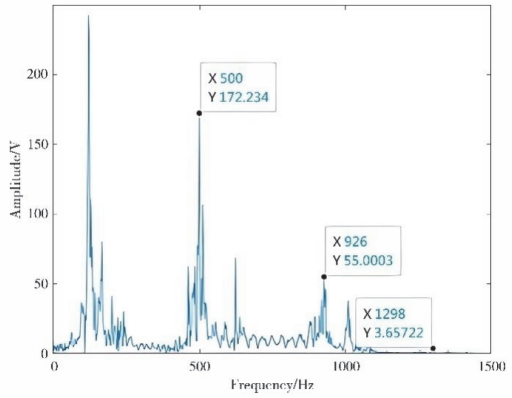

b. Spectrum diagram of signal after denoising

Figure 5 Comparison before and after denoising

The results indicate that maintaining noise-level-invariant threshold processing yields optimal denoising performance, as evidenced by both *SNR* and *MSE* metrics. As far as *SNR* and *MSE* are concerned, the optimal de-noising effect can be achieved by selecting the mode that the threshold processing does not change with the noise level, the decomposition scale is 1, the wavelet basis is db5, and the soft threshold function is combined with the wavelet parameters of sqtwolog rules. A visual representation comparing the signal before and after denoising is presented in the following figure.

By comparison of denoising results using image analysis, it becomes evident that the signal post-denoising exhibits enhanced clarity, smoother imagery, and a significant reduction in noise amplitude within both low-frequency and high-frequency bands. This observation leads to the conclusion that the denoising algorithm implemented in this study effectively reduces vibration amplitudes across both low- and high-frequency bands. Moreover, it demonstrates a commendable inhibitory effect on noise across both high and low frequencies, resulting in an overall strong denoising efficacy. This positive outcome is beneficial for advancing the accuracy of feature extraction in subsequent steps.

To evaluate the robustness and reliability of the proposed model, a triple cross-validation approach is employed with $k = 3$. The dataset is divided into three equal subsets, and for each fold, two subsets are used for training while the remaining subset serves as the test set. This process is repeated three times, ensuring that each subset is utilized as a test set exactly once. During each fold, the mean square error (*MSE*) is calculated to provide a comprehensive assessment of the model's performance. The results demonstrate consistent accuracy and robustness across all folds, verifying the model's generalization ability and reliability in vibration signal recognition tasks.

Table 3 Mean Square Error (*MSE*) Results for PSO-BP Model across Folds

PSO-BP species	*MSE* (mean square error)
1	0.062
2	0.094
3	0.125

3 FEATURE EXTRACTION

Following the denoising of pipeline vibration signals, a degree of redundancy remains in the denoised vibration signals. Therefore, it becomes imperative to extract features from these signals to reduce computational time. Vibration signals inherently comprise both time-domain and frequency-domain features [24]. Recognizing that a singular type of feature may not adequately characterize pipeline vibration signals, this study introduces three information entropy measures derived from the time-domain and frequency-domain features of the vibration signal. These entropies are fused to form the feature set of the pipeline vibration signal. Information entropy, with its capacity to characterize the degree of chaos stemming from uncertain factors in a system, is employed as a pivotal feature. Specifically, energy entropy is introduced as a reference feature within the information entropy feature vector, contributing positively to the realm of vibration recognition and classification [25]. Additionally, singular spectral entropy and power spectral entropy are integrated as additional features. The information entropy equation is outlined as follows:

$$H(x) = -\sum_{i=1}^{n} P(x)\log P(x) \tag{1}$$

where x is the energy of each IMF (intrinsic mode function). $P(x)$ is the ratio of energy per IMF (intrinsic mode function). $-P(x)\log P(x)$ is called CEE (energy entropy component). Each IMF is derived through empirical mode decomposition (EMD), which decomposes the original signal into multiple oscillatory components (IMFs) with different frequencies. The energy x of an IMF quantifies the contribution of that component to the overall signal.

Energy entropy is a representation of the complexity of signal energy, and the energy entropy equation is:

$$H_p = -\sum_{q=1}^{N} \varepsilon_{pq} \lg \varepsilon_{pq} \tag{2}$$

Among $\varepsilon_{pq}=E_{pq}/E_p$, where E_{pq} is the wavelet packet energy of the signal at the p-scale q time, $E_p$is the total signal energy of N sampling points at the p-scale.

Singular spectrum analysis of signals is a modern spectral analysis technique based on dynamic analysis, which can quantitatively describe the complex state characteristics of time series. The steps for calculation are as follows:

(1) Convert the original signal into matrix A.

(2) Perform singular value decomposition on matrix A to obtain the singular value spectrum.

(3) Calculate the proportion of each singular value to the sum of all singular values, and obtain the probability density function $P(x)$.

(4) Incorporate the probability density function into Eq. (1).

Power spectral entropy is used to represent the uncertainty of signal energy under power spectral partitioning and is a quantitative description of the complexity of signal energy distribution in the frequency domain. The steps for calculation are as follows:

(1) Finding the power spectrum of a signal.

(2) Calculate the proportion of energy in each frequency band to the total energy, and obtain the probability density function $P(x)$.

(3) Incorporate the probability density function into Eq. (1).

The eigenvalues are calculated using MATLAB, including maximum, minimum, mean, peak to peak, rectified mean, variance, standard deviation, kurtosis, skewness, root mean square, waveform factor, peak factor, pulse factor, margin factor, center of gravity, mean square frequency, root mean square frequency, frequency variance, frequency standard deviation, power spectral entropy, singular spectral entropy, and energy entropy, totaling 22 eigenvalues. The corresponding event types are stored in a table. Establish a model library for corresponding event types. The partial characteristic values of the signal are shown in Tab. 4, where event type 1 represents normal conditions, type 2 corresponds to vibration events, and Tn denotes the characteristic value type.

Table 4 Partial characteristic values of signals

	Pipeline normal signal	Pipeline normal signal	Pipeline normal signal	Pipeline vibration signal	Pipeline vibration signal
*T*1 (maximum value)	0.131	0.114	0.116	1.085	1.246
*T*4 (Peak value)	0.253	0.252	0.222	2.527	2.735
*T*6 (Standard deviation)	0.001	0.001	0.001	0.042	0.038
*T*8 (Root amplitude)	2.757	2.715	2.976	6.782	5.808
*T*10 (skewness)	0.033	0.0375	0.032	0.204	0.195
*T*22 (Energy entropy)	0.603	0.431	0.722	1.562	1.476

4 SIGNAL RECOGNITION

4.1. MATLAB Implementation of Correlation Analysis Feature Screening

Correlation analysis is generally the analysis of variables with correlation relationship, and the degree of correlation between variables is analyzed from a quantifiable point of view. The correlation coefficient is commonly used to measure the degree of correlation between two variables. The value of the correlation coefficient ranges from −1 to 1, where positive and negative values indicate the direction of change between the two variables, positive values represent the same direction of change, and negative values are opposite. Tab. 5 lists the correlation coefficients and the degree of correlation between variables.

Table 5 Correlation coefficient and correlation degree of variables

Coefficient range	Degree of variable correlation
0.0 - 0.2	Very weak correlation or no correlation
0.2 - 0.4	Weak correlation
0.4 - 0.6	Moderate correlation
0.6 - 0.8	Strong correlation
0.8 - 1.0	Most strong correlation

In this paper, Pearson correlation coefficient is calculated to describe the degree of correlation between two variables. The calculation formula is as follows.

$$\alpha = \frac{\sum_{i=1}^{n}\left(x_i-\bar{x}\right)\left(y_i-\bar{y}\right)}{\sqrt{\sum_{i=1}^{n}\left(x_i-\bar{x}\right)^2}\sqrt{\sum_{i=1}^{n}\left(y_i-\bar{y}\right)^2}} \tag{3}$$

This section utilizes 40 groups of denoised pipeline signal data, including 20 groups of pipeline vibration signals and 20 groups of normal pipeline signals. The eigenvalues calculated by each group of signals are labeled, the normal signal label is 1, and the vibration signal label is 2, resulting in a 23 × 40 matrix, where the first 22 rows correspond to eigenvalues for 22 features and the final row contains the labels, which is used as the unfiltered feature set. The algorithm for calculating Pearson correlation coefficient was implemented in MATLAB based on Eq. (4). The threshold of correlation coefficient is set to 0.54, and the Pearson correlation coefficient between the two variables of the characteristic value and the signal category is calculated. The result is presented in Fig. 6.

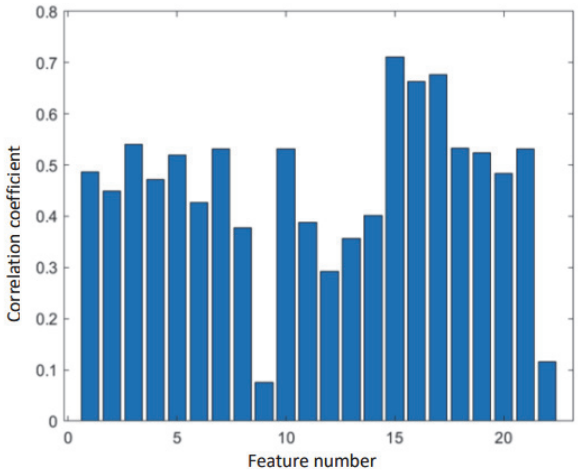

Figure 6 Correlation coefficient of eigenvalues

It can be seen from Fig. 6 that all feature values are positively correlated with signal categories. The feature with the largest correlation coefficient is numbered 15, which represents the gravity center frequency, and the feature with the smallest correlation coefficient is numbered 9, which represents the skewness. There are 4 features with correlation coefficient greater than 0.54, which are 3, 15, 16 and 17, respectively. Therefore, the features screened by correlation analysis are mean (3), barycentric frequency (15), mean square frequency (16) and root-mean-square frequency (17).

4.2. BP Neural Network

The BP neural network is a type of feedforward neural network that supports multi-parameter input and output [26]，Multi-parameter input and output means that when processing data, the system can accept multiple independent input variables and can produce multiple output results. BP neural network can learn complex function mapping based on multi-dimensional input features and output multi-dimensional results, which makes BP neural network can solve various complex practical problems. It has been widely applied. BP neural network structure refers to a multi-layer perceptron (MLP) network based on back propagation algorithm. The input layer of the BP neural network receives multiple input parameters. These input parameters are passed to the hidden layer for processing. The number of nodes in the input layer matches the number of input parameters. There can be one or more hidden layers, and each hidden layer contains several neurons. These neurons receive information from the input layer through weighted connections and apply the activation function for nonlinear transformation. The purpose of the hidden layer is to extract the advanced features of the input data. The output layer of the BP neural network produces the prediction results of the model. The number of nodes in the output layer matches the number of output parameters. For example, if the model needs to predict two output values, the output layer will have two nodes. Through its multi-layer structure, weight adjustment and activation function, BP neural network can effectively extract features from input parameters and transform these features into required output parameters. This structure

makes BP neural network perform well in dealing with complex tasks, such as image recognition, natural language processing and predictive analysis. The trained BP neural network can independently process nonlinear transformations with minimal output error for the input information of similar samples. BP neural network is a typical three-layer or multi-layer feedforward network with no feedback or intra layer interconnection structure [27]. The structure is shown in Fig.7.

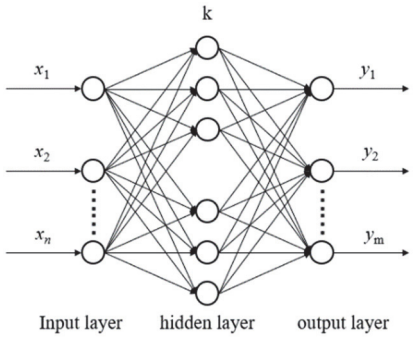

Figure 7 BP neural network structure

4.3 PSO-BP

The determination of the number of hidden nodes in a BP neural network is usually achieved through repeated forward and backward propagation, which affects the network's convergence and learning efficiency. To optimize the adjustment of weights and thresholds, as well as improve the learning efficiency and convergence speed of the network, a BP neural network model based on the PSO algorithm can be utilized, which belongs to a population-based swarm intelligence algorithm [28]. The PSO algorithm is inspired by the foraging behavior of bird flocks and fish schools. In the process of foraging, each individual in the group (referred to as a "particle") adjusts its position based on its own experience and that of its neighbors. These individuals find the food source through communication and cooperation, that is, the optimal solution of the problem. In PSO, each particle represents a potential solution in the solution space, and the particle swarm searches for the optimal solution through two main behaviors: individual behavior and social behavior. The PSO algorithm workflow typically involves initializing particle swarm, evaluating particle fitness, updating individual and global optimal solutions, and iterating. PSO algorithm can enhance the BP neural network by optimizing its initial weights and biases, avoiding local optimization, accelerating convergence and adaptive adjustment. PSO can evolve with random search by simulating biological activities. In the process of particle movement, the optimal solution is selected through local optimal and global optimal control, and a model is constructed. Each particle has adaptability determined by the model and a vector that decides the orientation and distance. Then, all particles collectively search for the optimal target value [29]. All particles represent a feasible solution to the optimization issue, which is calculated by the location and velocity of the particles [30]. When each particle discovers an optimal value, it updates its velocity and position using a specific Eq. [31].

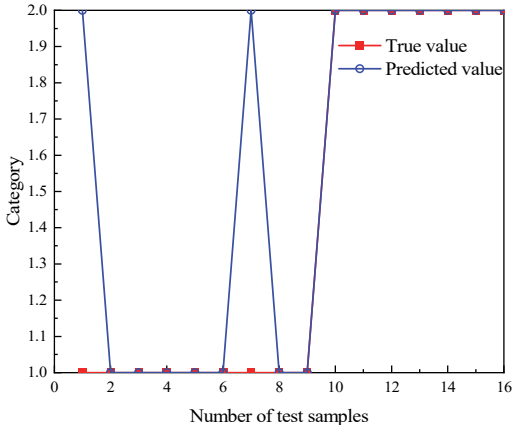

Figure 8 PSO-BP test results

According to the results in Fig. 8, among the 16 test samples, two samples were incorrectly identified. The accuracy was 87.5% and the *MSE* was 0.125. Compared to the unoptimized BP neural network (without PSO), the proposed method demonstrates significant improvements. The accuracy of the network's recognition of the test set was only 75%, and the *MSE* was 0.25. After optimization with PSO, the BP neural network demonstrates improved. The recognition accuracy of the model is significantly improved by 12.5 percentage points, and the *MSE* is reduced by 0.125. These results demonstrate that by optimizing the initial weights and thresholds of the BP neural network, the network performance has been significantly improved.

The bionic swarm intelligence algorithmic rule is used to construct the particle swarm intelligence procedure. This is based on random investigation and improved by exploitation. It tracks optimal solutions through collaboration and information sharing among individuals in the swarm. All particles represent a feasible solution to the optimization problem, which is calculated by the location and velocity of the particles. The ith particle's velocity and position are expressed by $vi = (vi1, vi2, vi3, vi4, \ldots, vim)$ and $pi = (pi1, pi2, pi3, pi4, \ldots, pim)$. Then, the latest position and velocity can be computed as Eq. (4) and Eq. (5).

$$v_{id}^{t+1} = \omega v_{id}^{t} + c_1 r_1 \left(p_{best} - p_{id}^{t} \right) + c_2 c_2 \left(g_{best} - p_{id}^{t} \right) \tag{4}$$

$$p_{id}^{t+1} = p_{id}^{t} + v_{id}^{t+1} \tag{5}$$

where v_{id} and p_{id} represent the velocity and position of the particles of generation d and generation i. t is the iteration number and ω is the inertia weight. c_1 and c_2 are constants, known as personal and social learning factors, respectively. r_1 and r_2 are two uniformly distributed random numbers generated independently within the range [0, 1]. p_{best} and g_{best} are the individual and population historical best solutions in generation d.

The flow chart of the BP neural network optimized using the PSO algorithm is shown in Fig.9.

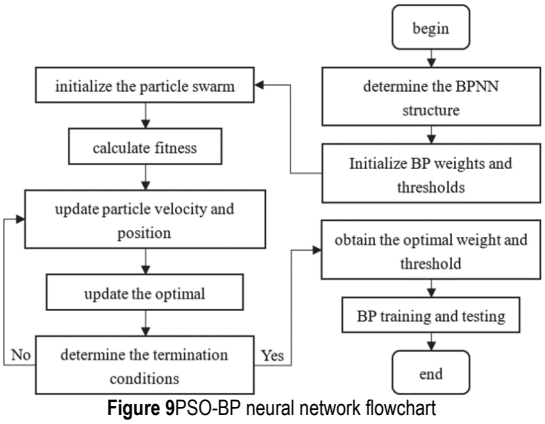

Figure 9PSO-BP neural network flowchart

4.4 Parameter Determination of the BP Neural Network

BP network requires the appropriate configuration of hidden layers and neurons. If there are too many hidden layers and neurons, it increases computational complexity and risks overfitting the network. On the other hand, if there are too few hidden layers and neurons, it results in inadequate training performance and underfitting the network [32]. The number of nodes in the hidden layer is usually obtained according to Eq. (6)

$$l=\sqrt{m+n}+a \tag{6}$$

Among them, m is the number of input layer nodes, n is the number of output layer nodes, and a *is a constant in the range* [1, 10].

Due to the small number of training samples, the number of hidden layers is set to 1. The learning rate is generally selected between 0.01 and 0.8, which determines the step size of weight updates. In this article, the learning rate is set to 0.1. The momentum coefficient is used to accelerate the process of weight update, which is set to 0.8 in this study.

The number of layers in the BP neural network is set to 3, the number of input layer nodes is 22 (i.e. 22 types of eigenvalues), and the number of hidden layer nodes is calculated based on empirical Eq. (5) to obtain 11 different node numbers within the range of [5, 15]. The network is run in stages and the number of nodes is selected by testing the sample mean square error. The results are shown in Tab. 6.

Table 6 Selection of Hidden Layer Nodes in BP Neural Network

Nodes	5	6	7	8	9	10	11	12	13	14	15
MSE	0.50	0.25	0.50	0.25	0.18	0.37	0.43	0.50	0.25	0.37	0.25

From the results in Tab. 5, the results in Tab. 5 indicate that 9 hidden layer nodes yield the optimal network model with the minimum *MSE*. Therefore, the number of hidden layer nodes is set to 9. The number of output layer nodes is 2. The BP neural network training method is the Levenberg Marquardt algorithm, utilizing the Levenberg-Marquardt algorithm for training, with the hidden layer employing the tansig activation function and the output layer using the purelin linear function.

4.5 Parameter Determination of PSO-BP Algorithm

The quality of particle position is determined by the fitness function. According to the problems and requirements of this paper, the fitness value is calculated based on the proportion of misclassified samples. The quality of particle positions is evaluated by calculating the error rate between the training simulation results and the category labels of the training samples. The smaller the fitness value, the better the particle position, the more accurate the training, and the better the effect. The equation for calculating the fitness function is as follows:

$$f=1-x/N \tag{7}$$

where x is the number of mismatches between the training simulation results and training samples, and N is the number of training samples.

$c1$ controls the degree to which particles search based on their own experience, and $c2$ controls the degree to which particles search based on group experience. When $c1$ is larger, the particles are more inclined to search according to their historical best position. However, if $c1$ is too large, it may cause the particle to fall into a local optimal solution and not be able to jump out. When $c2$ is large, the particle is more inclined to search according to the location of the global optimal solution, which helps the particle explore more widely in the search space and find a better solution. However, if $c2$ is too large, it may cause the particle to rely too much on the global optimal solution and overlook favorable local solutions. In general, $c1$ and $c2$ are between 0 and 2.

The selection of acceleration constants $c1$ and $c2$ has a direct impact on the performance of the PSO-BP neural network model. This study determines the coefficient sizes based on different ratios of $c1$ and $c2$, and the results are shown in Tab. 7. The particle swarm size was set to 20, the number of population updates to 50, and the maximum number of iterations to 1000, to achieve the goal of global search.

Table 7 R^2 size under different ratios of $c1$ and $c2$

$c1/c2$	$c1$	$c2$	$c1+c2$	R^2
0.5	1.333	2.667	4	0.778
2	2.667	1.333	4	0.779
0.75	1.714	2.286	4	0.838
4/3	2.286	1.714	4	0.766
1	2.000	2.000	4	0.863

The results show that when c1 is 1.714 and $c2$ is 2.286, the determination coefficient of PSO-BP neural network model is the largest and the model performance is the best. Therefore, $c1$ and $c2$ are set as 1.714 and 2.286 in the PSO-BP neural network model in this paper.

4.6 Model Evaluation

After the model training is completed, the effectiveness of the model needs to be evaluated. To make the evaluation more comprehensive, this study uses two performance indicators, determination coefficient (R^2) and mean square error (*MSE*), to comprehensively evaluate the network model established in this article. R^2 measures the goodness of fit for a model, with a range of values from negative infinity to 1; *MSE* is the average square of the difference between the predicted values of the model and the actual observed values; A closer R^2 value to 1 and a

smaller *MSE* indicate better network model performance.

The calculation equations are:

$$R^2 = 1 - \frac{\sum_{i=1}^{n}\left(y_i - y_i^{'}\right)^2}{\sum_{i=1}^{n}\left(y_i - \overline{y}\right)^2} \tag{8}$$

$$MSE = \frac{1}{N}\sum_{i=1}^{n}\left(y_i - y_i^{'}\right)^2 \tag{9}$$

Among them: N represents the number of samples $y_i, y_i^{'}, \overline{y}$ are the actual value, predicted value, and average value of the sample, respectively.

5 MODEL VALIDATION

5.1 Data Collection

The preprocessing steps consist of data cleaning, data standardization, data transformation, data integration, feature selection, feature construction and data segmentation.

The data was collected from a long-distance pipeline simulation experimental system that includes a 600 m long stainless-steel pipeline loop, 4 simulated pumping stations (a total of 8 pumps), 1 liquid storage tank, 1 gas storage tank, 1 air compressor, and corresponding power distribution and automation measurement and control systems. 40 sets of data were obtained through vibration tapping experiments, including two types of working conditions: normal and vibration. The simulation experimental device system for long-distance pipelines is shown in Fig.9.

Figure 9 Simulation experimental device system for long-distance pipelines

This study employs the wavelet threshold denoising method to preprocess it. To address parameter selection issues in the wavelet threshold denoising method, wavelet decomposition is performed to determine the appropriate scale range of the signal. Then, by evaluating the denoising performance of 63 different combinations of wavelet base and decomposition scale, the optimal wavelet base and decomposition scale are selected

The data acquisition setup comprises a 941B sensor, a D3000 data acquisition card, and a computer. Adhering to Nyquist's theorem, the sensor's sampling frequency is set at 20000 Hz.

The sensor and data acquisition card installed in the pipeline loop were used for data acquisition, and the number of samples was set to one-tenth of the acquisition frequency. The regulating valve of each station was manually adjusted to 100% opening, start the pump No. 1 - 4, after the medium in the pipeline is stable, the flow rate of each pump station is basically consistent, and the pressure in the pipeline remains constant, which is the normal operation condition of the pipeline. Pipe vibrations caused by third-party damage were simulated by knocking on the pipe in normal operating condition. The set sampling frequency and sampling number are not changed during data collection.

The sensor was strategically placed in the pipeline loop of the experimental device system and securely affixed with black insulation tape. To enhance signal authenticity and minimize the impact of uncertain factors, the sensor's contact surface with the pipeline is bonded with glue. Throughout the experiment, a stainless-steel centrifugal water pump served as the power source, with the water tank supplying the medium within the pipeline. The addition of a pressure regulating valve ensured the stable operation of the simulated experimental device system for long-distance pipelines. The collected pipeline's smooth and vibration signals were processed through a computer to serve as inputs for denoising algorithms.

5.2 System Sensitivity

To verify the system's sensitivity, this study collected signals by altering the positions of artificial tapping along the pipeline and analyzed the system's response under varying conditions. The experimental setup ensured stable operation of the pipeline loop, including a steady water source and calibrated signal acquisition equipment. Once the system and hardware stability were confirmed, sensitivity testing commenced. Three tapping points were established downstream of the sensor at distances of 3 meters, 5 meters, and 8 meters, labeled as Measuring Points 1, 2, and 3, respectively. At each measuring point, the tapping process was repeated 10 times to collect corresponding pipeline vibration signals. Additionally, to evaluate the potential impact of sensor location and fluid flow direction on the results, a control point was set upstream of the sensor at the same distance as Measuring Point 2 but in the opposite direction. All collected data were stored in the database, properly categorized, and marked for seamless analysis in the signal recognition module.

The experimental results showed that the system maintained a high classification accuracy of over 89% across all measuring points, indicating strong system reliability. Specifically, the average classification accuracy and Signal-to-Noise Ratio (*SNR*) for Measuring Point 1 were 94.5% and 9.2 dB, respectively. Measuring Point 2 yielded an accuracy of 92.3% and an *SNR* of 8.8 dB, while Measuring Point 3 recorded an accuracy of 89.7% and an *SNR* of 7.9 dB. The control point results were similar to Measuring Point 2, with an accuracy of 91.2% and an *SNR* of 8.5 dB. A slight decline in classification accuracy and *SNR* was observed as the tapping distance increased, likely due to signal attenuation over longer distances. However, the control point results indicated that fluid flow direction

had minimal influence on system performance.

These findings validate the system's sensitivity and adaptability. The multi-point experimental design effectively assessed the system's response to changes in tapping locations while also accounting for potential interference from factors such as fluid flow direction. The results demonstrate that the proposed method exhibits strong robustness and application potential under complex operating conditions. The arrangement of measuring points is shown in Fig. 10.

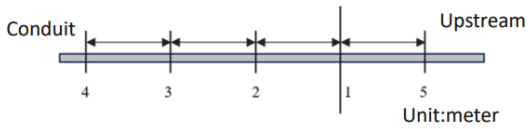

Figure 10 Station diagram

After logging in to the system and entering the signal recognition interface, users can access the database in the lower-left corner of the interface to select data for analysis. Then, users can sequentially import collected signal data into the signal recognition module for processing and analysis. Tab. 7 lists the detection results.

Table 7 Detection result

Measuring point	Tapping position	Number of knocks	Recognize the correct frequency
*L*1	0m	0	9
*L*2	3m	10	10
*L*3	5m	10	10
*L*4	8m	10	9
*L*5	3m	10	10

According to the experimental statistical results in Table 6, the following conclusions can be drawn:

(1) For the signals collected at different locations of the sensor, the system achieved an identification accuracy rate exceeding 95%. By comparing the recognition results of *L*2 and *L*5 measurement points, it can be seen that the recognition performance of the system is not affected by the flow direction of the fluid in the pipeline.

(2) At measuring points *L*2 and *L*3 located downstream of the pipeline and *L*5 located upstream of the pipeline, the system can correctly identify signals. This shows that the arrangement of measuring points does not influence experimental outcomes. However, at the position of 0 meters and 8 meters from the sensor, there is a signal recognition error, which may be related to the accuracy of the sensor and the force of the human percussion.

(3) The system successfully implemented pipeline signal detection, demonstrating high accuracy and reliability, thereby verifying its sensitivity.

5.3 Network Model Training

Denoising and feature extraction were performed on the 40 sets of data obtained from the experiment and obtained 40 sets of feature sets as training samples. The input of the network is 22 types of feature values from the feature set, that is, building 22 × 9 × 1 network topology. Among them, 24 feature sets are used as training samples, and 16 sets of feature sets are used as testing samples.

To mitigate calculation errors from varying data units and system errors from factor magnitude differences, the input and output data are normalized before presenting the training patterns to the network [33]. It uses the following equation to normalize the data:

$$Y = \frac{(X - X_{\min})}{(X_{\max} - X_{\min})} \tag{9}$$

In the equation: Y represents the normalized input data; X is the measured data; $X_{\min}$, $X_{\max}$ are the maximum and minimum values in the measured data, respectively.

Two types of networks were trained with the 40 feature sets, and the evaluation metrics obtained are shown in Fig. 11 and Fig. 12.

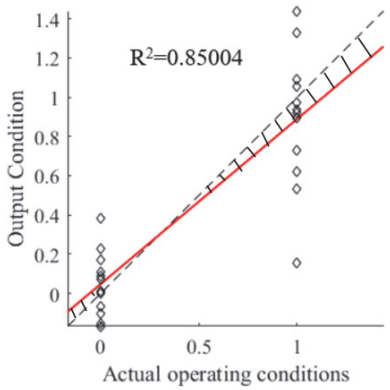

Figure 11 Overall recognition of BP training samples

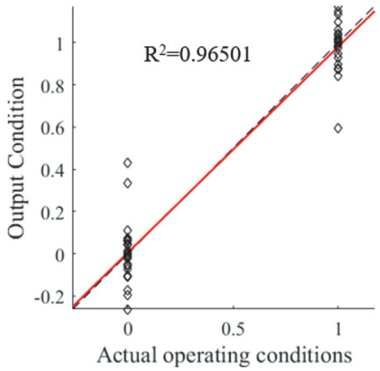

Figure 12 Overall recognition of PSO-BP training samples

Table 8 Performance comparison of two network models

	R^2	*MSE*
BP	0.85	0.187
PSO-BP	0.96	0.062
Difference value of BP and PSO-BP	−0.11	0.125

5.4 Result Analysis

Tab. 8 reveals that, in comparison to traditional BP neural networks, PSO-BP neural networks achieve smaller Mean Squared Error (*MSE*), higher recognition accuracy, and R^2. This signifies that during the model training process, the output values of PSO-BP neural networks align more closely with the actual values of the training samples, indicating enhanced classification abilities. When considering the same sample size, as depicted in Fig. 9 and Fig. 10, it becomes evident that the fitting degree R^2 between the output value and the actual value of the PSO-BP neural network surpasses that of the BP neural network by 13.53%.

This points towards superior model performance, heightened accuracy, and a reduced overall relative error for the PSO-BP neural network. Through this analysis, it can be concluded that the PSO-BP neural network model proposed in this study effectively performs classification and recognition of pipeline vibration signal conditions [34]. Furthermore, it demonstrates superior classification accuracy and generalization ability compared to traditional BP neural networks. This is illustrated in Fig. 13.

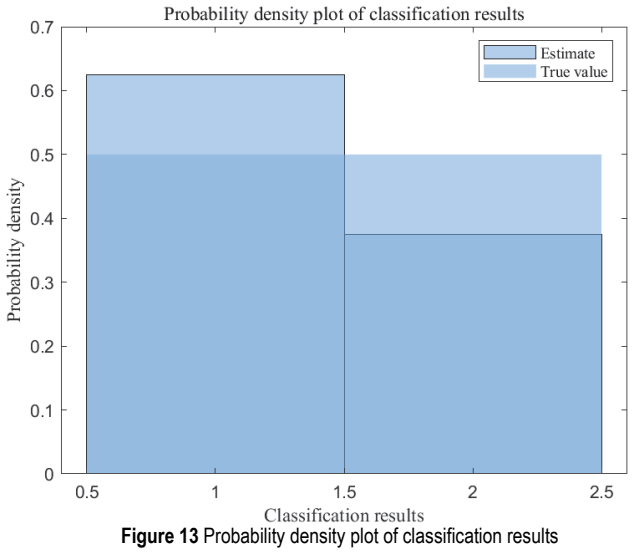

Figure 13 Probability density plot of classification results

6 CONCLUSION

The author warrants that the article is original, written by stated author/s, has not been published before and it will not be submitted anywhere else for publication prior to acceptance by TEHNIČKI VJESNIK/ TECHNICAL GAZETTE (TV), contains no unlawful statements, does not infringe the rights of others, and that any necessary written permissions to quote from other sources have been obtained by the authors.

This article proposes a new wavelet parameter selection method, which employs a fixed threshold to address noise level variations. In our experiment, the conditions for collecting data include defining experimental parameters, standardizing operation procedures, using calibrated equipment, controlling environmental conditions, recording detailed information, repeating experiments and synchronizing data. Before applying the proposed method, the preprocessing steps consist of data cleaning, data standardization, data transformation, data integration, feature selection, feature construction and data segmentation. By following the above data collection conditions and pretreatment steps, the repeatability and data quality of experimental results can be significantly improved, thus ensuring the effectiveness and accuracy of subsequent analysis. These techniques may not work well in specific types of pipe materials or geological conditions, or may not be suitable for detecting certain types of damage.

At the same time, hardware limitations, environmental factors, sensor accuracy and reliability may also affect the performance of the algorithm in field applications. Firstly, the wavelet basis and decomposition scale with the best noise effect are selected, and then the threshold processing pattern with noise level changes is changed to select the threshold denoising method and threshold selection rule combination with the best noise effect. Finally, the optimal parameter combination for denoising pipeline vibration signals was selected through comparison. Compared to traditional manual experimental selection of wavelet parameters, the parameter selection method proposed in this paper is more efficient and reasonable, greatly reducing screening time and making it easier to obtain the best combination of wavelet parameters for denoising. The PSO algorithm is introduced to optimize their parameter configuration, which improves the accuracy and efficiency of the recognition algorithm. Through the prior data verification, the recognition algorithm suitable for pipeline vibration signal is successfully verified, which ensures the high performance and reliability of the system.

Using an improved PSO-BP neural network model, a total of 22 eigenvalues including maximum value, kurtosis, skewness, energy entropy, etc. were selected as input parameters, and event type was used as output parameter. The network topology structure established through analysis was 22 × 9 × 2. The *MSE* of the model validation result is 6.2%, which is much better than the optimal result of 18.7% validated by the BP neural network. The verification results indicate that the improved PSO algorithm optimized BP neural network model has better classification ability and can be effectively applied in practical engineering to classify the types of events that occur in pipelines.

The effective combination of wavelet threshold denoising method and BP neural network optimized using the PSO algorithm has been achieved. This method significantly outperforms traditional methods in both recognition accuracy and model performance, while fully improving signal restoration. After evaluating the denoising effect of 63 combinations of wavelet bases and decomposition scales, the best denoising effect of wavelet base and decomposition scale is determined. In addition, through comparative analysis, the optimal threshold function and threshold selection rules are determined, which provides a solid technical basis for the subsequent signal processing.

Acknowledgements

This research is supported by Fujian Provincial Science and Technology Department Guiding Project (2022H0032). All support is gratefully acknowledged.

7 REFERENCES

[1] Woldesellasse, H. &Tesfamariam S. (2023). Risk analysis of onshore oil and gas pipelines: Literature review and bibliometric analysis. *Journal of Infrastructure Intelligence and Resilience,2*(4), 100052. https://doi.org/10.1016/j.iintel.2023.100052

[2] Hong, B., Shao, B., Guo, J., Fu, J., Li, C., & Zhu, B. (2023). Dynamic Bayesian network risk probability evolution for third-party damage of natural gas pipelines. *Applied Energy,333*, 120620. https://doi.org/10.1016/j.apenergy.2022.120620

[3] Herdovics, B. & Cegla, F. (2020). Long-term stability of

guided wave electromagnetic acoustic transducer systems. *Structural health monitoring, 19*(1), 3-11. https://doi.org/10.1177/1475921718805733

[4] Peng, L., Huang, S., Wang, S., & Zhao, W. (2021). A Simplified Lift-Off Correction for Three Components of the Magnetic Flux Leakage Signal for Defect Detection. *IEEE Transactions on Instrumentation and Measurement, 70*, 1-9. https://doi.org/10.1109/TIM.2021.3058407

[5] Rukhshinda, W., Mohammad, O. T., Gholamhossein, S., Ryan, M., & John, R. (2022). Development of Permanently Installed Magnetic Eddy Current Sensor for Corrosion Monitoring of Ferromagnetic Pipelines. *Applied Sciences, 12*(3), 1037. https://doi.org/10.3390/app12031037

[6] Bui Quy, T. & Kim, J. (2020). Leak detection in a gas pipeline using spectral portrait of acoustic emission signals. *Measurement, 152*, 107403. https://doi.org/10.1016/j.measurement.2019.107403

[7] Wook, J. H., Lee, H., & Hwang, I. (2023). Supervised learning-based classification of acoustic emission and vibration signal for identifying condition change of district heating system. *Measurement, 220*, 113388. https://doi.org/10.1016/j.measurement.2023.113388

[8] Huang, S., Peng, L., Sun, H., & Li, S. (2023). Deep Learning for Magnetic Flux Leakage Detection and Evaluation of Oil & Gas Pipelines: A Review. *Energies, 16*(3), 1372. https://doi.org/10.3390/en16031372

[9] Wencheng, W., Yang, Y., Xiaobao, Y., Vikash, V. G., Yunpeng, W., Jinjun, T., & Zhenzhou, Y. (2024). A Negative Binomial Lindley Approach Considering Spatiotemporal Effects for Modeling Traffic Crash Frequency with Excess Zeros. *Accident Analysis and Prevention, 207*(2024), 107741. https://doi.org/10.1016/j.aap.2024.107741

[10] Saritha, C., Sukanya, V., & Narasimha Murthy, Y. (2008). ECG Signal Analysis Using Wavelet Transforms. *Bulg. J. Phys.2008*, 31-35.

[11] Oran Brigham, E. (1988). The Fast Fourier Transform and its Applications. *Prentice-Hall, Inc.*

[12] Portnoff, M. (1980). Time-Frequency Representation of Digital Signals and Systems Based on - Short-Time Fourier Analysis.*Ieee Trans Acoust Speech Signal Process, 1980*, 21-28. https://doi.org/10.1109/TASSP.1980.1163359

[13] Halidou, A., Mohamadou, Y., Ari, A. A. A., & Zacko, E. J. G. (2023). Review of wavelet denoising algorithms. Multimedia Tools and Applications, *82*(27), 41539-41569. http://doi.org/10.1007/s11042-023-15127-0

[14]Naqiuddin, M. S. M., Leong, M. S., Hee, L. M., & Azrieasrie, M. A. M. (2019). Ultrasonic signal processing techniques for Pipeline: A review. *Matec Web of Conferences, 255*, 6006. http://doi.org/10.1051/matecconf/201925506006

[15] Qiu, C., Zhao, B., Liu, S., Zhang, W., Zhou, L., Li, Y., & Guo, R. (2023). Data Classification and Demand Prediction Methods Based on Semi-Supervised Agricultural Machinery Spare Parts Data. *Agriculture, 13*(1), 49. https://doi.org/10.3390/agriculture13010049

[16] Liu, X., Zhao, D., Peng, Y., & Li, J. (2023). A Wavelet Basis ANN and 5-Class Decision Factor AI Algorithm. *International Journal of Pattern Recognition and Artificial Intelligence, 37*(08) https://doi.org/10.1142/S0218001423590176

[17] Derong, K. & Jixuan, M. (2023). Radar Signal Classification System Based on BP Neural Network. *Academic Journal of Engineering and Technology Science, 6*(1) http://doi.org/10.25236/AJETS.2023.060110

[18] Yang, Y, Yin, Y, Wang, Y. P., Meng, R., & Yuan, Z. (2023). Modeling of Freeway Real-Time Traffic Crash Risk Based on Dynamic Traffic Flow Considering Temporal Effect Difference. *Journal of Transportation Engineering Part A Systems, 149*(7), 04023063. https://doi.org/10.1061/JTEPBS.TEENG-7717

[19] Jiang, W., Ding, W., Zhu, X., & Hou, F. (2022). A Recognition Algorithm of Seismic Signals Based on Wavelet Analysis. *Journal of Transportation Engineering Part A Systems, 10*(8), 1093. https://doi.org/10.3390/jmse10081093

[20] Li, H. & Wang, J. (2022). Based on Wavelet Threshold Denoising-LDA and Bilstm Aircraft Engine Life Prediction. *Journal of physics. Conference series*, *2410*(1), 12019. https:/doi:10.1088/1742-6596/2410/1/012019

[21] Guo, Y., Zhou, X., Li, J., Ba, R., Xu, Z., Tu, S., & Chai, L. (2023). A Novel and Optimized Sine−Cosine Transform Wavelet Threshold Denoising Method Based on the sym4 Basis Function and Adaptive Threshold Related to Noise Intensity. *Applied Sciences, 13*(19), 10789. https://doi.org/10.3390/app131910789

[22] Oouyang, C., Cai, L., Liu, B., & Zhang, T. (2023). An improved wavelet threshold denoising approach for surface electromyography signal.*EURASIP Journal on Advances in Signal Processing, 2023*(1). https://doi.org/10.1186/s13634-023-01066-3

[23] Gao, J. & Zhang, X. (2023). An Information Recognition and Time Extraction Method of Tracking a Flying Target with a Sky Screen Sensor Based on Wavelet Modulus Maxima Theory. *Mathematics, 11*(18), 3936. https://doi.org/10.3390/math11183936

[24] Yang, Y., Yang, B., Yuan, Z., Meng, R., & Wang, Y. (2024). Modeling and Comparing Two Modes of Sharing Parking Spots at Residential Area: Real-time and Fixed-time Allocation. *IET Intelligent Transport Systems, 18*(4). https://doi.org/10.1049/itr2.12343

[25] Ma, H., Li, X., Liu, Q., Xingbo, Xie., Ji, C., & Zhao, C. (2020). Research on Identification Technology of Explosive Vibration Based on EEMD Energy Entropy and Multiclassification SVM. *Shock and Vibration, 2020*(2), 1-10. https://doi.org/10.1155/2020/7893925

[26] Peng, W., Jiang, W., Yang, B., Sun, G., & Shao, X. (2023). An indentation method for measuring welding residual stress: Estimation of stress-free indentation curve using BP neural network prediction model. *International Journal of Pressure Vessels and Piping, 206*, 105070. https://doi.org/10.1016/j.ijpvp.2023.105070

[27] Chen, H., Miao, Y., Chen, Y., Fang, L., Zeng, L., & Shi, J. (2021). Intelligent Model-based Integrity Assessment of Nonstationary Mechanical System. *Journal of Web Engineering, 2021*(1). https://doi.org/10.13052/jwe1540-9589.2022

[28] Zhang, Y., Zhao, D., He, L., Zhang, Y., & Huang, J. (2024). Research on prediction model of electric vehicle thermal management system based on particle swarm optimization-Back propagation neural network. *Thermal Science and Engineering Progress, 47*, 102281. https://doi.org/10.1016/j.tsep.2023.102281

[29] Liu, K. & Su, H. (2023). Optimization of the BP neural network for Wind Power Output Prediction Based on Particle Swarm Optimization Algorithm. *Journal of physics. Conference series, 2562*(1), 12010. https://doi.org/10.1088/1742-6596/2562/1/012010

[30] Karthika, S. & Rathika, P. (2024). An adaptive data compression technique based on optimal thresholding using multi-objective PSO algorithm for power system data. *Applied Soft Computing, 150*, 111028. https://doi.org/10.1016/j.asoc.2023.111028

[31] Tan, J., Hu, H., Liu, S., Chen, C., & Xuan, D. (2022). Optimization of PEMFC system operating conditions based on neural network and PSO to achieve the best system performance. *International Journal of Hydrogen Energy, 47*(84), 35790-*35809.* https://doi.org/10.1016/j.ijhydene.2022.08.154

[32] Wang Z, JiW, Zhao, T., Wu, Q., Liu, P., & Wang, T. (2024). Efficient inverse design method of AWG based on BPNN-

PSO algorithm. *Optics Communications, 552*, 130080. https://doi.org/10.1016/j.optcom.2023.130080

[33] Zhong, W. L., Ding, H., Zhao, X., & Fan, F.L. (2023). Mechanical properties prediction of geopolymer concrete subjected to high temperature by BP neural network. *Construction and Building Materials, 409*, 133780. https://doi.org/10.1016/j.conbuildmat.2023.133780

[34] Lu, J., Chai, Y., Hu, Z. et al. (2024). A novel image denoising algorithm and its application in UAV inspection of oil and gas pipelines. *Multimed Tools Appl*, 83, 34393-34415. https://doi.org/10.1007/s11042-023-16752-5

Contact information:

Fang WANG, Senior engineer
(Corresponding author)
Fujian Boiler and Pressure Vessel Inspection and Research Institute
NO. 370 Lubin Road,
Cangshan District, Fuzhou 350008, Fujian Province, China
E-mail: wangfang2080@163.com

Caijun XU, Senior engineer
Fujian Boiler and Pressure Vessel Inspection and Research Institute
NO. 370 Lubin Road,
Cangshan District, Fuzhou 350008, Fujian Province, China
E-mail: fjtjxucaijun@163.com

Bin LIU, associate professor
Shijiazhuang Tiedao University,
Shijiazhuang, Hebei 050043, China
No.17, North Second Ring East Road
Shijiazhuang 050043, Hebei Province, China
E-mail: liubin@stdu.edu.cn

Wenjun CHEN, Master Degree Candidate
Shijiazhuang Tiedao University,
Shijiazhuang, Hebei 050043, China
No.17, North Second Ring East Road
Shijiazhuang 050043, Hebei Province, China
E-mail: cwj992271633@163.com

Shaodong YAN, Master Degree Candidate
Shijiazhuang Tiedao University,
Shijiazhuang, Hebei 050043, China
No. 17, North Second Ring East Road
Shijiazhuang 050043, Hebei Province, China
E-mail: hxy992271633@163.com